
LEARNING WITHOUT FEEDBACK: DIRECT RANDOM TARGET PROJECTION AS A FEEDBACK-ALIGNMENT ALGORITHM WITH LAYERWISE FEEDFORWARD TRAINING

Charlotte Frenkel^{*†}

ICTEAM Institute
Université catholique de Louvain
Louvain-la-Neuve BE-1348, Belgium
charlotte.frenkel@uclouvain.be

Martin Lefebvre^{*}

ICTEAM Institute
Université catholique de Louvain
Louvain-la-Neuve BE-1348, Belgium
martin.lefebvre@uclouvain.be

David Bol

ICTEAM Institute
Université catholique de Louvain
Louvain-la-Neuve BE-1348, Belgium
david.bol@uclouvain.be

ABSTRACT

While the backpropagation of error algorithm allowed for a rapid rise in the development and deployment of artificial neural networks, two key issues currently preclude biological plausibility: (i) symmetry is required between forward and backward weights, which is known as the weight transport problem, and (ii) updates are locked before both the forward and backward passes have been completed. There is thus a growing interest in the development of training algorithms that release these constraints and ensure locality in both parameters and error signals while minimizing the training performance penalty. The feedback alignment (FA) algorithm uses fixed random feedback weights and shows that the network learns to align its forward and backward weights to maximize error gradient information. The direct feedback alignment (DFA) variation directly propagates the output error to each hidden layer through fixed random connectivity matrices. In this work, we show that using only the error sign is sufficient to maintain feedback alignment and to provide learning in the hidden layers. As in classification problems the error sign information is already contained in the targets (i.e. one-hot-encoded labels), using the latter as a proxy for the error brings three advantages: (i) it solves the weight transport problem by eliminating the requirement for an explicit feedback pathway, which also reduces the computational workload, (ii) it reduces memory requirements by removing update locking, allowing for weight updates to be computed in each layer independently without requiring a full forward pass, and (iii) it leads to a purely feedforward and low-cost algorithm that only requires a label-dependent random vector selection to estimate the layerwise loss gradients. Therefore, in this work, we propose the direct random target projection (DRTP) algorithm and demonstrate on the MNIST and CIFAR-10 datasets that, despite the absence of an explicit error feedback, DRTP performance can still lie close to the one of BP, FA and DFA. The low memory and computational cost of DRTP and its reliance only on layerwise feedforward computation make it suitable for deployment in adaptive edge computing devices.

Index terms – Neural networks, deep learning, backpropagation, feedback alignment, local learning, random feedback, hardware-oriented learning, biologically-plausible plasticity.

^{*}These authors contributed equally.

[†]C. Frenkel is with Université catholique de Louvain as a Research Fellow from the National Foundation for Scientific Research (FNRS) of Belgium.

1. Introduction

Artificial neural networks (ANNs) were proposed as a first step toward bio-inspired computation by emulating the way the brain processes information with densely-interconnected neurons and synapses as computational and memory elements, respectively [1, 2]. In order to train ANNs, it is necessary to identify how much each neuron contributed to the output error, a problem referred to as *credit assignment* [3]. The backpropagation of error algorithm (BP) [4] allowed solving the credit assignment problem for multi-layer ANNs, thus enabling the development of deep networks for applications ranging from computer vision (e.g., [5, 6, 7]) to speech recognition (e.g., [8, 9]). However, two critical issues preclude BP from being biologically plausible.

First, BP requires symmetry between the forward and backward weights, which is known as the *weight transport problem* [10]. Beyond implying a perfect and instantaneous communication of parameters between the feedforward and feedback pathways, error backpropagation requires each layer to have full knowledge of all the weights in the downstream layers, making BP a non-local algorithm for both weight and error information. Therefore, there is an increasing interest in developing training algorithms that release the weight symmetry constraint, as it has been shown that weight symmetry is not mandatory to reach near-BP performance [11]. The feedback alignment (FA) algorithm [12], also called random backpropagation in [13], demonstrates that using fixed random weights in the feedback pathway allows conveying useful error gradient information, as the network learns to align the forward weights with the backward ones. Direct feedback alignment (DFA) [14] builds on these results and directly propagates the error between the network predictions and the targets to each hidden layer through fixed random connectivity matrices. DFA demonstrates a limited accuracy penalty compared to BP on the MNIST [15] and CIFAR-10 [16] datasets, while using the output error as a global modulator and keeping weight information local. Therefore, DFA bears important structural similarity with learning rules that are believed to take place in the brain, known as three-factor synaptic plasticity rules [17], which rely on local pre-synaptic and post-synaptic spike-based activity together with a global modulator. This similarity was leveraged in [18] and [19], where direct adaptations of DFA as a biologically-plausible spike-based learning rule are proposed. The BP, FA and DFA algorithms are summarized in Figs. 1a-1c, respectively.

The second issue of BP is its requirement for a full forward pass before parameters can be updated during the backward pass, a phenomenon referred to as *update locking* in [20, 21]. Beyond making BP biologically implausible, update locking has critical implications for BP implementation as it requires buffering all the layer inputs and activations during the forward and backward passes in order to compute the weight updates, leading to a high memory overhead. As the previously-described FA and DFA solutions to the weight transport problem only tackle the weight locality aspect, specific techniques enabling local error handling or gradient approximation are required to tackle update locking. On the one hand, the error locality approach relies on layerwise loss functions [22, 23, 24], it enables training layers independently and without requiring a forward pass in the entire network. In [22], local errors are generated using auxiliary fixed random classifiers and allow for near-BP performance on the MNIST and CIFAR-10 datasets. This strategy has been ported in [23] to a biologically-plausible spike-based three-factor synaptic plasticity rule. In [24], it is shown that a combination of two layerwise loss functions enables scaling to ImageNet [25] without compromising performance. However, these approaches still suffer from update locking at the layer scale as single-layer forward and backward passes are required. In [22], Mostafa *et al.* also investigate the weight transport problem, however weight symmetry is only partially relaxed: in order to maintain performance, it is necessary to keep at least the weight sign information during the backward pass in the auxiliary fixed random classifiers. On the other hand, the synthetic gradients approach proposed in [20, 21] relies on layerwise predictors of subsequent network computation. However, training local gradient predictors still require backpropagating gradient information from deeper layers. Finally, the approach pursued in [26] defines layerwise target values, relying on auto-encoders at each layer. However, as these layerwise target values are still generated sequentially, this approach fails at solving the update locking problem [20].

In order to fully solve both the weight transport and the update locking problems, we propose the direct random target projection (DRTP) algorithm (Fig. 1d). Compared to DFA, the targets (i.e. one-hot-encoded labels) are used in place of the output error and projected onto the hidden layers. We demonstrate both theoretically and experimentally that, in the framework of classification problems, the error sign information contained in the targets is sufficient to maintain feedback alignment between the estimated loss gradients δz_k for the weighted sum of inputs in layer k , denoted as the *modulatory signals* in the subsequent text, and allows training multi-layer networks, leading to three key advantages. First, DRTP solves the weight transport problem by entirely removing the need for dedicated feedback pathways. Second, layers can be updated independently and without update locking as a full forward pass is not required, thus reducing memory requirements by releasing the need to buffer inputs and activations of each layer. Third, DRTP is a purely feedforward and low-cost algorithm whose updates rely on layerwise information that is immediately available upon computation of the layer outputs. Estimating the layerwise loss gradients δy_k only requires a label-dependent random vector selection, contrasting with the error locality and synthetic gradients approaches that require the addition

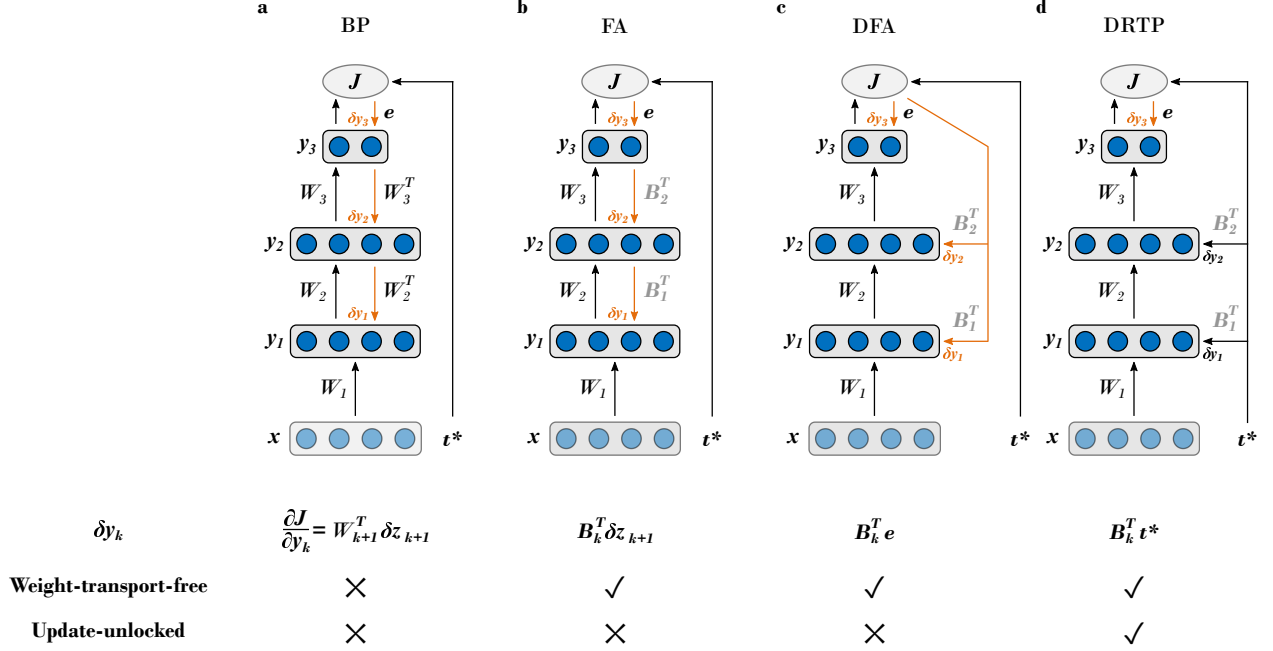


Figure 1: The proposed direct random target projection algorithm builds on feedback-alignment-based algorithms to tackle the weight transport problem while further releasing update locking. Black arrows indicate the feedforward pathways and orange arrows the feedback pathways. In the k -th layer, the weighted sum of inputs y_{k-1} is denoted as z_k and the activation function as $f_k(\cdot)$, with $k \in [1, K]$ and K the number of layers. Trainable forward weight matrices are denoted as W_k and fixed random connectivity matrices as B_k . The input vector is denoted as x , the target vector as t^* and the loss function as $J(\cdot)$. The estimated loss gradients for the outputs of the k -th hidden layer, denoted as δy_k , are provided for each training algorithm, where the modulatory signals are defined as $\delta z_k = \delta y_k \odot f'_k(z_k)$, with \odot denoting the elementwise multiplication operator. **(a)** Backpropagation of error algorithm (BP) [4]. **(b)** Feedback alignment (FA) algorithm [12]. **(c)** Direct feedback alignment (DFA) algorithm [14]. **(d)** Proposed direct random target projection (DRTP) algorithm. Adapted from [14, 21].

of side networks for error or gradient prediction. DRTP even compares favorably to DFA, as the latter still requires a multiplication between the output error and a fixed random matrix.

DRTP allows relaxing structural, memory and computational requirements, yet we demonstrate on the MNIST and CIFAR-10 datasets that DRTP performance can still lie close to the one of BP, FA and DFA. Therefore, DRTP is ideal for implementation in edge computing devices, enabling adaptation to uncontrolled environments while meeting stringent power and resource constraints. Suitable applications thus range from distributed smart sensor networks for the Internet-of-Things (IoT) [27] to embedded systems and cognitive robotic agents [28]. DRTP can also be formulated as a three-factor learning rule for biologically-plausible learning and embedded neuromorphic computing, in which high-density synaptic plasticity can currently not be achieved without compromising learning performance [29, 30].

2. Results

2.1. Weight updates based only on the error sign provide learning to multi-layer networks

We demonstrate with two experiments, respectively on a regression task and a classification problem, that modulatory signals based only the error sign are within 90° of those prescribed by BP, thus providing learning in multi-layer networks. To do so, we use an error-sign-based version of DFA, subsequently denoted as sDFA, in which the error vector is replaced by the error sign in the global feedback pathway.

2.1.1. Regression

This first experiment aims at demonstrating that the error sign provides useful modulatory signals to multi-layer networks by comparing training algorithms on a regression task. The objective is to approximate 10 nonlinear functions

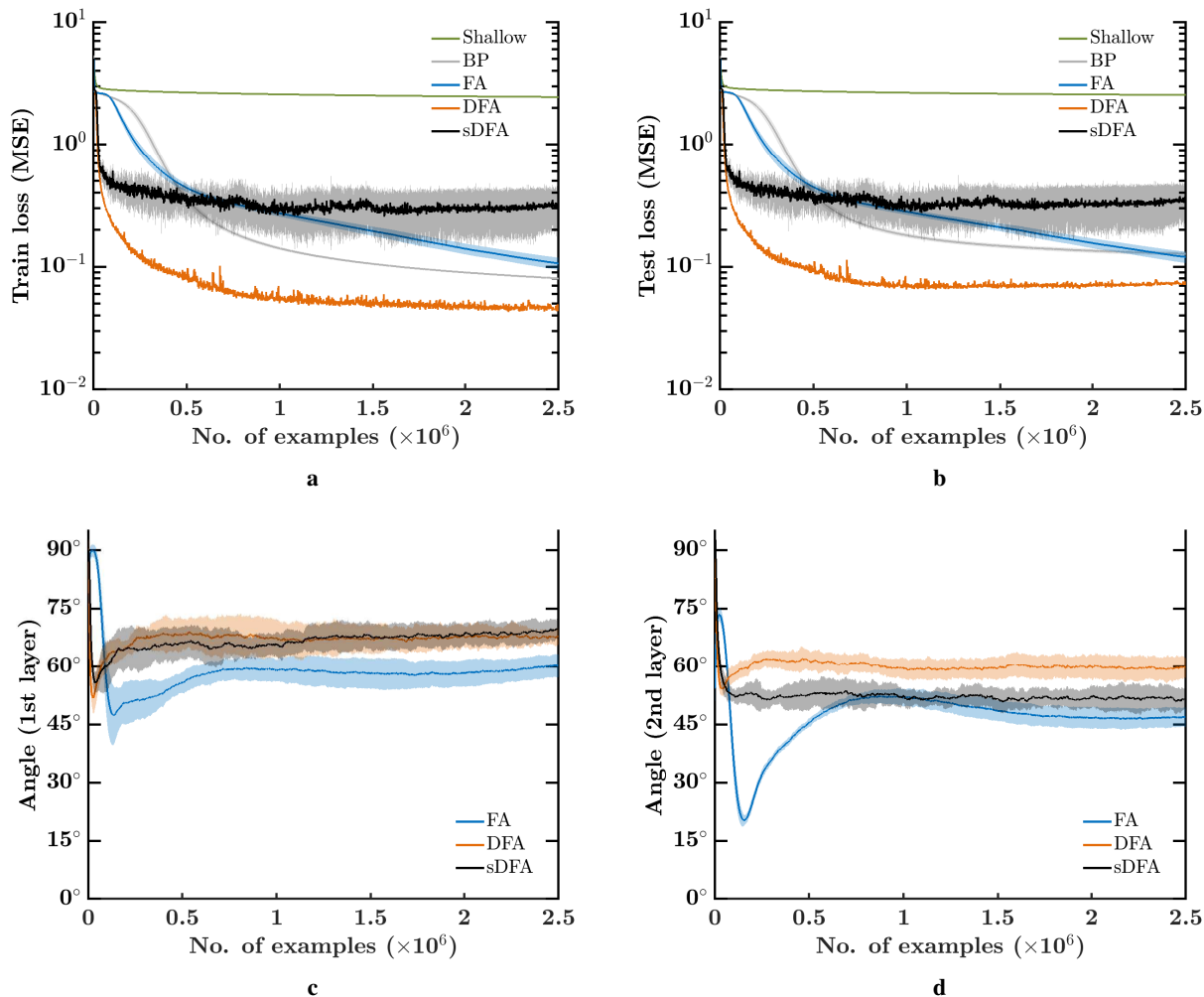


Figure 2: Error-sign-based direct feedback alignment (sDFA) provides useful modulatory signals in regression tasks. A 256-100-100-10 network with tanh hidden and output units is trained to learn cosine functions with five training algorithms: shallow learning, BP, FA, DFA and sDFA. As for other feedback-alignment-based algorithms, sDFA updates are within 90° of the backpropagation updates. The train and test losses and the alignment angles are monitored every 1k samples, error bars are one standard deviation over 10 runs. Angles have been smoothed by an exponentially-weighted moving average filter with a momentum coefficient of 0.95. **(a)** Mean squared error loss on the 5k-example training set. **(b)** Mean squared error loss on the 1k-example test set. **(c)** Angle between the modulatory signals δz_k prescribed by BP and by feedback-alignment-based algorithms in the first hidden layer. **(d)** Angle between the modulatory signals δz_k prescribed by BP and by feedback-alignment-based algorithms in the second hidden layer.

$T_j(x) = \cos(\bar{x} + \phi_j)$, where $\phi_j = -\pi/2 + j\pi/9$ for $j \in [0, 9]$ and \bar{x} denotes the mean of x , a 256-dimensional vector whose entries are drawn from a normal distribution with a mean lying in $[-\pi, \pi]$ (Section 4). A 256-100-100-10 fully-connected network is trained to approximate $T(\cdot)$ with five training algorithms: shallow learning (i.e. frozen random hidden layers and trained output layer), BP, FA, DFA and sDFA.

The mean squared error (MSE) loss on the training set is shown in Fig. 2a. While shallow learning fails to learn a meaningful approximation of $T(\cdot)$, sDFA and DFA show the fastest initial convergence, which is a consequence from the separate direct feedback pathway precluding gradients from vanishing. While DFA demonstrates the highest performance on this task, sDFA comes earlier to stagnation as it does not account for the output error magnitude reduction as training progresses, thus depriving a reduction of the effective learning rate in the hidden layers as the output error decreases. sDFA would therefore benefit from the use of a learning rate scheduler. Similar conclusions hold for the loss on the test set (Fig. 2b). The angle between the modulatory signals prescribed by BP and by feedback-alignment-based algorithms is shown in Figs. 2c and 2d, for the first and second hidden layers, respectively. While all feedback-alignment-based algorithms lie close to each other within 90° of the BP modulatory signals, FA has a clear advantage during the first 100 epochs on the 5k-example training set. sDFA performs on par with DFA in the first hidden layer, while it surprisingly provides a better alignment than DFA in the second hidden layer, though not fully leveraged due to the absence of modulation in the magnitude of the updates from the output error.

2.1.2. Classification

With this second experiment, we demonstrate that, in addition to providing useful modulatory signals for regression problems, the error sign information allows training multi-layer networks to solve classification problems. The task consists in training a 256-500-500-10 network to solve a synthetic classification problem with 16×16 -pixel images and 10 classes; the data to classify is generated automatically with the Python `skLearn` library (see Section 4). As for regression, the network is trained with shallow learning, BP, FA, DFA and sDFA.

Fig. 3a shows that, after 500 epochs with a 25k-example training set, DFA provides the fastest and most accurate training with a misclassification rate of 0.05%, followed by BP, FA and sDFA with 0.19%, 0.64% and 1.54%, respectively. Shallow learning lags almost an order of magnitude behind with 8.95%. However, Fig. 3b shows that DFA also has a higher overfitting and lies close to sDFA on the test set, with 3.48% and 4.07%, respectively. The lowest misclassification rates are of 1.85% for BP and 1.81% for FA, while shallow learning lags behind at 9.57%. The angle between the modulatory signals prescribed by BP and by feedback-alignment-based algorithms is shown in Figs. 3c and 3d, for the first and second hidden layers, respectively. As for the regression task in Section 2.1.1, all feedback-alignment-based algorithms exhibit alignments close to each other. Here, alignments tend to level off after 50 epochs, with the lowest angle provided by FA, followed by DFA and sDFA. As sDFA is always within 90° of the BP modulatory signals, it is able to train multi-layer networks.

2.2. For classification, a feedback pathway is no longer required as the error sign is known in advance

In the framework of classification problems, training examples (x, c^*) consist of an input data sample to classify, denoted as x , and a label c^* denoting the class x belongs to, among C possible classes. The target vector, denoted as t^* , corresponds to the one-hot-encoded class label c^* . The output layer nonlinearity is conventionally chosen as a sigmoid or softmax function, yielding output values that are strictly bounded between 0 and 1. Denoting the output vector of a K -layer network as y_K , the error vector is defined as $e = y_K - t^*$. Under the aforementioned conditions, it results that an entry e_c of the C -dimensional error vector e is defined as

$$e_c = \begin{cases} y_{Kc} - 1 & \text{if } c = c^*, \\ y_{Kc} & \text{otherwise.} \end{cases}$$

As the entries of y_K are strictly bounded between 0 and 1, the error sign is given by

$$\text{sign}(e_c) = \begin{cases} -1 & \text{if } c = c^*, \\ 1 & \text{otherwise.} \end{cases}$$

Due to the nonlinearity in the output layer forcing the output values to remain bounded between 0 and 1, the error sign is class-dependent and known in advance as training examples (x, c^*) already provide the error sign information with the label c^* . A feedback pathway is thus no longer required as it has been shown that the error sign allows providing useful modulatory signals to train multi-layer networks (Section 2.1). Therefore, beyond being free from the *weight transport problem* as DFA, sDFA also releases *update locking* and the associated memory overhead in classification problems.

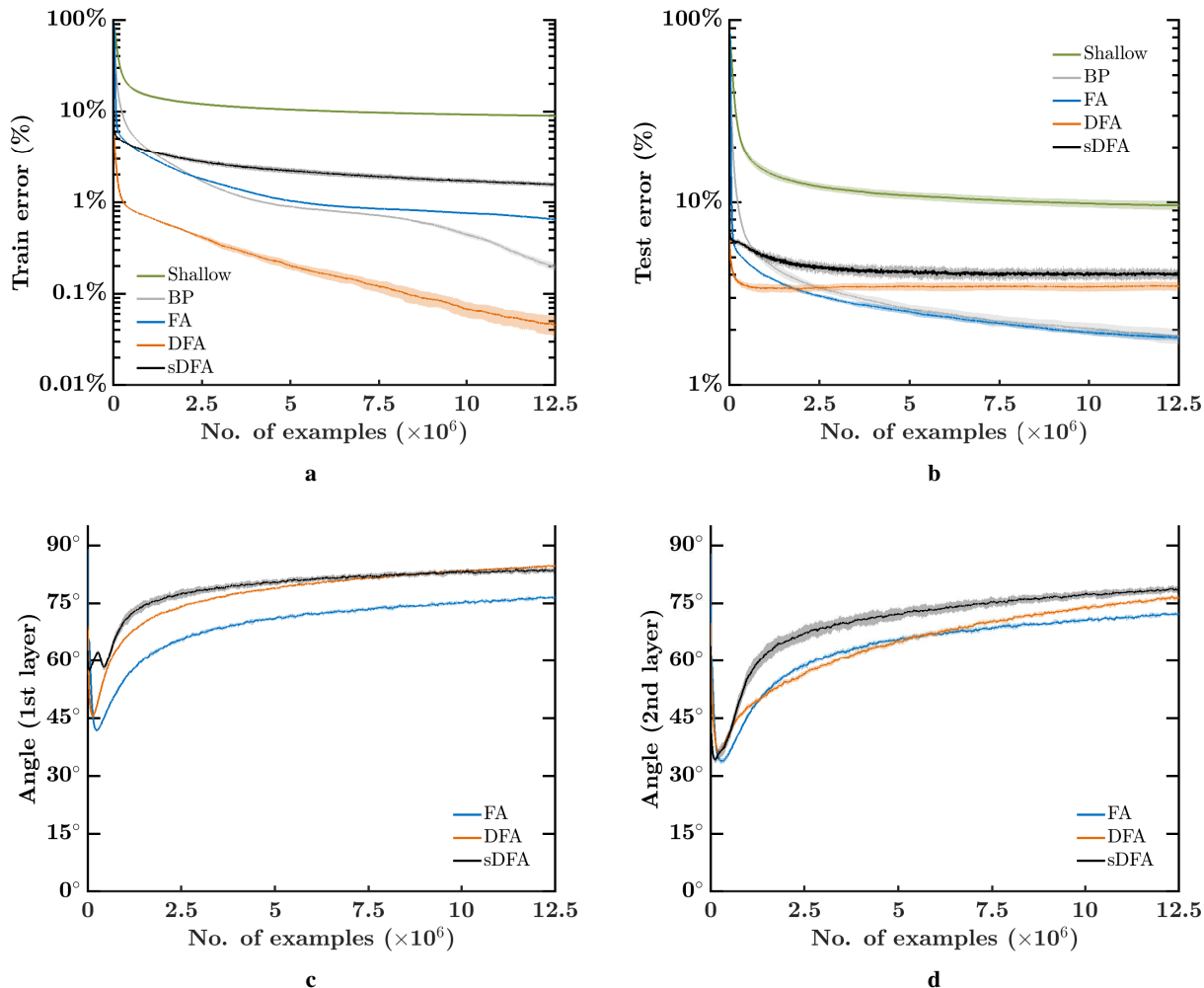


Figure 3: Error-sign-based direct feedback alignment (sDFA) provides useful modulatory signals in classification tasks. A 256-500-500-10 network with tanh hidden units and sigmoid output units is trained to classify a synthetic dataset of 16×16 -pixel images into 10 classes with five training algorithms: shallow learning, BP, FA, DFA and sDFA. The update directions of the sDFA algorithm are within 90° of the backpropagation updates and are comparable to other feedback-alignment-based algorithms. The train and test losses and the alignment angles are monitored every 2.5k samples, error bars are one standard deviation over 10 runs. Angles have been smoothed by an exponentially-weighted moving average filter with a momentum coefficient of 0.95. **(a)** Error on the 25k-example training set, reaching on average 0.19% for BP, 0.64% for FA, 0.05% for DFA, 1.54% for sDFA and 8.95% for shallow learning after 500 epochs. **(b)** Error on the test set, reaching on average 1.85% for BP, 1.81% for FA, 3.48% for DFA, 4.07% for sDFA and 9.57% for shallow learning after 500 epochs. **(c)** Angle between the modulatory signals δz_k prescribed by BP and by feedback-alignment-based algorithms in the first hidden layer. **(d)** Angle between the modulatory signals δz_k prescribed by BP and by feedback-alignment-based algorithms in the second hidden layer.

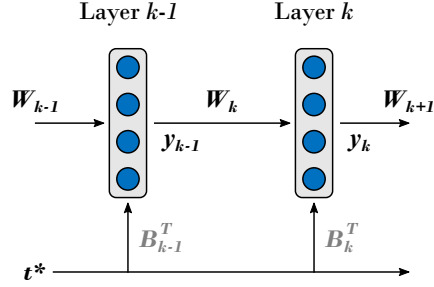


Figure 4: Network of DRTP-updated linear hidden layers considered in the context of the mathematical proof of alignment between the DRTP and BP modulatory signals. The same conventions as in Fig. 1 are used.

2.3. Direct random target projection delivers useful modulatory signals for classification

This section aims at providing the grounds to show why the proposed direct random target projection (DRTP) algorithm delivers useful modulatory signals to multi-layer networks in the framework of classification problems. First, we show how DRTP can be viewed as a simplified version of sDFA in which the target vector t^* is used as a surrogate for the error sign. Next, we demonstrate mathematically that, in a multi-layer network composed of a linear hidden layers and of a nonlinear output layer, the modulatory signals prescribed by DRTP and BP are always within 90° of each other, thus providing learning in multi-layer networks.

DRTP is a simplified version of error-sign-based DFA. As it has been shown in Section 2.2 that sDFA both solves the *weight transport* and the *update locking* problems in classification tasks, we propose the direct random target projection (DRTP) algorithm as a simplified version of sDFA while enhancing both performance and computational efficiency. In sDFA, the feedback signal randomly projected to the hidden layers is the sign of the error vector $e = y_K - t^*$, while in DRTP, this feedback signal is replaced by the target vector t^* . Being a one-hot encoding of c^* , t^* has a single positive entry corresponding to the correct class and zero entries elsewhere:

$$t_c^* = \frac{1 - \text{sign}(e_c)}{2} = \begin{cases} 1 & \text{if } c = c^*, \\ 0 & \text{otherwise.} \end{cases}$$

Thus, t^* corresponds to a surrogate for the error sign vector used in sDFA, where shift, rescaling and sign inversion operations have been applied to $\text{sign}(e)$. As the connectivity matrices B_k in the DRTP δy_k gradients $B_k^T t^*$ are fixed and random (Fig. 1d), they can be viewed as comprising the sign inversion and rescaling operations. Only the shift operation applied to $\text{sign}(e)$ makes a critical difference between DRTP and sDFA, which is favorable to DRTP for two reasons. First, DRTP is computationally cheaper than sDFA. Indeed, projecting the target vector t^* to the hidden layers through fixed random connectivity matrices is equivalent to a label-dependent selection of a layerwise random vector. On the contrary, sDFA requires a matrix product between the error sign vector and the fixed random connectivity matrices for each training example, as all entries of the error sign vector are non-zero. Second, experiments on the MNIST and CIFAR-10 datasets show that DRTP systematically outperforms sDFA (Supplementary Figs. 1a and 2a). Indeed, when the feedback information only relies on the error sign and no longer on its magnitude, the weight updates become less selective to the useful information: as all entries of the error sign vector have unit norm, the $C - 1$ entries corresponding to incorrect classes outweigh the single entry associated to the correct class and degrade the alignment (Supplementary Figs. 1b and 2b).

The directions of the DRTP and BP modulatory signals are within 90° of each other. We provide a mathematical proof of alignment between the DRTP and BP modulatory signals. The structure of our proof is inspired from the FA proof of alignment in [12], which we expand in two ways. First, we extend this proof for the case of DRTP. Second, while [12] demonstrates the alignment with the BP modulatory signals for a network consisting of a single linear hidden layer, a linear output layer and a mean squared error loss, we demonstrate that alignment can be achieved for an arbitrary number of linear hidden layers, a nonlinear output layer with sigmoid activation and a binary cross-entropy loss for classification problems. Both proofs are restricted to the case of a single training example. Under these specific conditions, it is possible to guarantee that the DRTP modulatory signals are aligned with those of BP. This comes from the fact that the prescribed weight updates lead to a soft alignment between the product of forward weight matrices and the fixed random connectivity matrices. The mathematical details, including the lemma and theorem proofs, have been abstracted out to Supplementary Note 1.

In the case of the multi-layer neural network composed of linear hidden layers shown in Fig. 4, the output of the k -th hidden layer is given by

$$y_k = z_k = W_k y_{k-1} \quad \text{for } k \in [1, K-1],$$

where K is the number of layers and $y_0 = x$ is the input vector. The output layer is described by

$$\begin{aligned} z_K &= W_K y_{K-1} \\ y_K &= \sigma(z_K), \end{aligned}$$

where σ is the sigmoid activation function. The loss function $J(\cdot)$ is the binary cross-entropy loss, computed over the C output classes:

$$J(y_K, t^*) = -\frac{1}{C} \sum_{c=1}^C \left(t_c^* \log(y_{Kc}) + (1 - t_c^*) \log(1 - y_{Kc}) \right).$$

Lemma. In the case of zero-initialized weights, i.e. $W_k^0 = 0$ for $k \in [1, K]$, and hence of zero-initialized hidden layer outputs, i.e. $y_k^0 = 0$ for $k \in [1, K-1]$ and $z_K^0 = 0$, considering a DRTP-based training performed recursively with a single element of the training set (x, c^*) and t^* denoting the one-hot encoding of c^* , at every discrete time step t , there are positive scalars $s_{y_k}^t$ and $s_{W_k}^t$ for $k \in [1, K-1]$ and a C -dimensional vector $s_{W_K}^t$ such that

$$\begin{aligned} y_k^t &= -s_{y_k}^t (B_k^T t^*) & \text{for } k \in [1, K-1] \\ W_1^t &= -s_{W_1}^t (B_1^T t^*) x^T \\ W_k^t &= s_{W_k}^t (B_k^T t^*) (B_{k-1}^T t^*)^T & \text{for } k \in [2, K-1] \\ W_K^t &= -s_{W_K}^t (B_{K-1}^T t^*)^T. \end{aligned}$$

Theorem. Under the same conditions as in the lemma and for the linear-hidden-layer network dynamics described above, the k -th layer modulatory signals prescribed by DRTP are always a positive scalar multiple of the Moore-Penrose pseudo-inverse of the product of forward matrices of layers $k+1$ to K , located in the feedback pathway between the output layer and the k -th hidden layer, multiplied by the error. That is, for $k \in [1, K-1]$ and $t > 0$,

$$\left(\prod_{i=k+1}^K W_i^t \right)^+ e = s_k^t B_k^T t^* \quad \text{with } s_k^t > 0.$$

Alignment. In the framework of classification problems, as the coefficients s_k^t are strictly positive scalars for $t > 0$, it results from the theorem that the dot product between the BP and DRTP modulatory signals is strictly positive, i.e.

$$\begin{aligned} e^T \left(\prod_{i=k+1}^K W_i^T \right)^T (B_k^T t^*) &> 0 \\ e^T \underbrace{\left(\prod_{i=k+1}^K W_i^T \right)^T \left(\prod_{i=k+1}^K W_i \right)^+}_{I} \frac{e}{s_k^t} &> 0 \\ \frac{e^T e}{s_k^t} &> 0. \end{aligned}$$

The BP and DRTP modulatory signals are thus within 90° of each other. \square

2.4. DRTP learns to classify MNIST and CIFAR-10 images without feedback

In this section, we compare DRTP with BP and other feedback-alignment-based algorithms, namely FA and DFA, on the MNIST and CIFAR-10 datasets. Both datasets have 10 output classes and respectively consist in classifying 28×28 greyscale images of handwritten digits for MNIST and 32×32 RGB images of vehicles and animals for CIFAR-10. The network topologies considered in our experiments are, on the one hand, fully-connected (FC) networks with one or two hidden layers, each hidden layer being constituted of either 500 or 1000 tanh units. On the other hand, convolutional (CONV) networks are used with either fixed random or trainable kernels (Section 4).

Network		BP	FA	DFA	DRTP
FC1-500	DO 0.0	1.72±0.08%	1.92±0.08%	2.59±0.11%	4.58±0.12%
	DO 0.1	1.55±0.03%	1.66±0.06%	2.17±0.10%	4.65±0.13%
	DO 0.25	1.64±0.06%	1.73±0.05%	2.32±0.08%	5.36±0.11%
FC1-1000	DO 0.0	1.76±0.06%	1.90±0.06%	2.12±0.05%	4.03±0.13%
	DO 0.1	1.58±0.03%	1.63±0.03%	1.82±0.04%	4.00±0.13%
	DO 0.25	1.70±0.06%	1.65±0.05%	1.88±0.05%	4.59±0.07%
FC2-500	DO 0.0	1.62±0.12%	1.95±0.07%	4.35±0.30%	4.57±0.13%
	DO 0.1	1.61±0.05%	1.62±0.06%	3.17±0.33%	4.76±0.11%
	DO 0.25	1.84±0.05%	1.77±0.07%	3.10±0.29%	5.77±0.12%
FC2-1000	DO 0.0	1.67±0.07%	1.90±0.07%	3.46±0.25%	4.04±0.12%
	DO 0.1	1.85±0.06%	1.63±0.05%	2.39±0.13%	4.03±0.09%
	DO 0.25	2.31±0.06%	1.69±0.04%	2.34±0.12%	4.86±0.06%
CONV (random)	DO 0.0	1.31±0.08%	1.55±0.04%	1.66±0.11%	1.87±0.12%
	DO 0.1	2.32±0.74%	1.43±0.05%	1.77±0.16%	2.11±0.15%
	DO 0.25	2.22±0.33%	1.39±0.04%	1.96±0.23%	2.59±0.19%
CONV (trained)	DO 0.0	0.99±0.05%	1.38±0.06%	2.38±0.39%	1.81±0.14%
	DO 0.1	0.97±0.04%	1.23±0.05%	2.62±0.57%	1.79±0.16%
	DO 0.25	2.18±0.07%	1.18±0.05%	2.68±0.36%	2.10±0.21%

Table 1: Mean and standard deviation of the test error on the MNIST dataset over 10 trials. DO stands for dropout and indicates the dropout probability used in the fully-connected layers of both FC and CONV networks. The FC networks consist of one (FC1) or two (FC2) hidden layers comprising 500 or 1000 tanh units, with an output fully-connected layer of 10 units. The CONV network topology is as follows: a convolutional layer with 32 5×5 kernels, a stride of 1 and a padding of 2, a max-pooling layer with 2×2 kernels and a stride of 2, a fully-connected layer of 1000 tanh units and an output fully-connected layer of 10 units.

2.4.1. MNIST

The results on the MNIST dataset are summarized in Table 1. Without dropout, the DRTP mean test error is within 3% of BP, 2.7% of FA and 2% of DFA for FC networks and within 0.9% of BP, 0.5% of FA and 0.2% of DFA for CONV networks, demonstrating that DRTP successfully learns to classify MNIST digits without feedback. It can be observed that dropout has no significant positive impact on DRTP, while a moderate dropout probability of 0.1 exhibits the best results for BP, FA and DFA in FC networks. The change of network topology that most decreases the error is the use of CONV networks, highlighting that extracting spatial redundancy information, even with random kernels, is a key to solve the MNIST task. All training algorithms nearly perform on par with fixed random kernels. BP is able to take the most out of trainable kernels, followed by FA, DRTP mostly stagnates while DFA incurs an accuracy penalty. This is due to the fact that there is not enough parameter redundancy in convolutional layers to allow for an efficient training with feedback-alignment-based algorithms. Indeed, the angle between the BP loss gradients and the feedback-alignment-based ones is roughly 90° , leading to random updates (Supplementary Fig. 3). The same effect explains why increasing the number of hidden units in fully-connected layers helps decreasing the error of all feedback-alignment-based algorithms, especially for DFA and DRTP, as it increases parameter redundancy.

2.4.2. CIFAR-10

The results on the CIFAR-10 dataset are summarized in Table 2. Without dropout, the DRTP mean test error is within 5.5% of BP and 4.5% of FA and DFA for FC networks and within 2.6% of BP, 2.4% of FA and 2.3% of DFA for CONV networks with fixed random kernels, demonstrating that DRTP also successfully learns to classify CIFAR-10 images without feedback. If the kernels are made trainable, the accuracy of BP is improved by approximately 3%, while FA only slightly improves and DFA and DRTP are negatively impacted, resulting from the low parameter redundancy in convolutional layers. Regarding dropout, both moderate and large dropout probabilities (DO 0.1 and DO 0.25) work fairly well for BP, FA and DFA. However, for DRTP, only a moderate dropout probability (DO 0.1) is able to improve the classification accuracy. Finally, data augmentation (DA) is effective in improving the performance of all algorithms and, in the case of DRTP, is more effective than dropout.

Network		BP	FA	DFA	DRTP
FC1-500	DO 0.0	48.43±0.30%	49.59±0.25%	49.73±0.24%	53.72±0.30%
	DO 0.1	47.57±0.38%	48.70±0.27%	48.98±0.23%	53.55±0.29%
	DO 0.25	47.97±0.22%	48.63±0.21%	48.52±0.19%	54.33±0.22%
	DA	45.78±0.35%	47.07±0.30%	47.28±0.41%	52.76±0.16%
FC1-1000	DO 0.0	47.58±0.21%	48.56±0.28%	48.45±0.17%	52.99±0.22%
	DO 0.1	46.50±0.26%	47.71±0.22%	47.64±0.31%	52.89±0.31%
	DO 0.25	46.17±0.22%	47.08±0.17%	48.22±3.36%	53.32±0.28%
	DA	44.74±0.24%	46.17±0.25%	46.16±0.24%	51.99±0.30%
FC2-500	DO 0.0	49.23±0.24%	50.83±0.20%	50.76±0.24%	53.46±0.16%
	DO 0.1	46.43±0.36%	48.86±0.24%	49.42±0.36%	53.59±0.29%
	DO 0.25	45.32±0.32%	47.81±0.28%	48.00±0.31%	54.52±0.22%
	DA	46.58±0.36%	48.75±0.27%	48.60±0.19%	52.53±0.41%
FC2-1000	DO 0.0	49.00±0.22%	50.35±0.18%	50.51±0.24%	52.83±0.44%
	DO 0.1	45.71±0.22%	47.91±0.24%	48.54±0.09%	52.49±0.19%
	DO 0.25	43.52±0.36%	45.66±0.30%	46.51±0.36%	53.51±0.42%
	DA	46.01±0.24%	47.80±0.22%	48.01±0.23%	51.48±0.39%
CONV (random)	DO 0.0	30.13±0.31%	30.28±0.37%	30.40±0.46%	32.69±0.38%
	DO 0.1	29.58±0.36%	29.45±0.35%	29.85±0.26%	32.77±0.50%
	DO 0.25	29.43±0.48%	30.69±0.34%	29.67±0.18%	33.86±0.54%
	DA	28.39±0.22%	28.39±0.24%	28.80±0.40%	31.01±0.28%
CONV (trained)	DO 0.0	27.45±0.28%	29.84±0.31%	32.06±0.29%	35.45±0.76%
	DO 0.1	26.41±0.25%	28.89±0.41%	30.75±0.39%	35.69±0.45%
	DO 0.25	24.73±0.21%	29.18±0.50%	29.68±0.43%	35.63±0.66%
	DA	25.36±0.29%	28.19±0.34%	30.34±0.49%	34.89±0.50%

Table 2: Mean and standard deviation of the test error on the CIFAR-10 dataset over 10 trials. DO stands for dropout and indicates the dropout probability used in the fully-connected layers of both FC and CONV networks. DA stands for data augmentation, which consists in horizontal flipping of the training images. No dropout is used for DA. The FC networks consist of one (FC1) or two (FC2) hidden layers comprising 500 or 1000 tanh units, with an output fully-connected layer of 10 units. The CONV network topology is as follows: two convolutional layers with respectively 64 and 256 3×3 kernels, a stride and a padding of 1, both followed by a max-pooling layer with 2×2 kernels and a stride of 2, then two fully-connected layers of 1000 tanh units and an output fully-connected layer of 10 units.

3. Discussion

While the backpropagation of error algorithm allowed taking artificial neural networks to outperform humans on complex datasets such as ImageNet [31], the key problems of *weight transport* and *update locking* highlight how aiming at breaking accuracy records on standard datasets has led to leave aside hardware efficiency considerations. While accuracy is the key driver for applications that can be backed by significant GPU and CPU resources, the development of decentralized adaptive smart sensors calls for keeping hardware requirements of learning algorithms to a minimum. Moreover, it has been shown that weight transport and update locking preclude biological plausibility [10, 13], following from the non-locality in both weight and gradient information. Therefore, there is currently an increasing interest in releasing these constraints in order to achieve higher hardware efficiency and to understand the mechanisms that could underlie biological synaptic plasticity.

The DRTP algorithm that we propose successfully addresses both the weight transport and the update locking problems, which has only been partially demonstrated in previously-proposed approaches. Indeed, the FA and DFA algorithms only address the weight transport problem [12, 14]. The error locality approach still suffers from the weight transport problem in the local classifiers [22, 23, 24], while the synthetic gradients approach requires backpropagating gradient information from deeper layers in order to train the layerwise gradient predictors [20, 21]. Both the error locality and the synthetic gradients approaches also incur computational overhead by requiring the addition of side local networks for error or gradient prediction. On the contrary, DRTP is a strikingly simple rule that alleviates the two key BP issues by enabling each layer to be updated with local information as the forward evaluation proceeds. In order to estimate the

layerwise loss gradients δy_k for each layer, the only operation required by DRTP is a label-dependent random vector selection (Fig. 1d). Despite the absence of dedicated feedback pathways and its low computational and memory costs, we demonstrated on the MNIST and CIFAR-10 datasets that DRTP performance still lies close to the one of BP, FA and DFA, thus highlighting its suitability for deployment in adaptive smart sensors at the edge and embedded systems.

By solving the weight transport and update locking problems, DRTP also releases key biological implausibility issues. Neurons in the brain separate forward and backward information in somatic and dendritic compartments, a property that is highlighted in the formulation of three-factor synaptic plasticity rules [17]: pre-synaptic and post-synaptic activities are modulated by a third factor corresponding to a local dendritic voltage. Lillicrap *et al.* build on the idea that a separate dendritic compartment integrates higher-order feedback and generates local teaching signals, where the errors could be viewed as a mismatch between expected and actual perceptions or actions [12]. This aspect is further emphasized in the subsequent work of Guerguiev *et al.* when framing DFA as a spike-based three-factor learning rule [18]. In the case of DRTP, compared to DFA, the error signal is replaced by the targets, which could correspond to a modulation that bypasses the actual perceptions or actions, relying only on predictions. Understanding the mechanisms of synaptic plasticity is critical in the field of neuromorphic engineering, which aims at porting biological computational principles to hardware toward higher energy efficiency [32, 33]. However, even simple local bio-inspired learning rules such as spike-timing-dependent plasticity (STDP) [34] can lead to non-trivial hardware requirements, which currently hinders adaptive neuromorphic systems from reaching high-density large-scale integration [29]. While adaptations of STDP, such as spike-dependent synaptic plasticity (SDSP) [35], release most of the STDP hardware constraints, their training performance is currently not sufficient to support deployability of neuromorphic hardware for real-world scenarios [29, 30]. A three-factor formulation of DRTP would release the update locking problem in the spike-based three-factor formulations of DFA [18, 19], which currently imply memory and control overhead in their hardware implementations [36, 37]. Porting DRTP to neuromorphic hardware is thus the subject of our future work.

Finally, while DRTP relaxes structural, memory and computational requirements toward decentralized hardware deployment, the accuracy penalty over DFA, although limited, comes from the fact that only the error sign is taken into account, not its magnitude. This aspect could be mitigated by keeping track of the error magnitude over the last samples in order to modulate the layerwise learning rates, at the expense of releasing the purely feedforward nature of DRTP. Otherwise, as outlined in Section 2.1.1, a fixed learning rate scheduler can be used. As for all other feedback-alignment-based algorithms, DRTP does not improve or even slightly degrades accuracy when applied to convolutional layers. Convolutional layers do not provide the parameter redundancy that can be found in fully-connected layers, a *bottleneck effect* that was first highlighted for FA in [12] and has recently been studied for DFA in [38]. If fixed random convolutional layers do not meet the performance requirements of the target application, a combination of DRTP for fully-connected layers together with error locality or synthetic gradients approaches for convolutional layers can be considered. This granularity in the selection of learning mechanisms, trading off accuracy and hardware efficiency, comes in accordance with the wide spectrum of plasticity mechanisms that are believed to operate in the brain [39].

4. Methods

The training on both the synthetic regression and classification tasks and the MNIST and CIFAR-10 datasets has been carried out with PyTorch [40], one of the numerous Python frameworks supporting deep learning. The PyTorch code allowing to reproduce our experiments can be found at <https://github.com/ChFrenkel/DirectRandomTargetProjection>.

Regression. The examples in the training and test sets are denoted as (x, t^*) . The 10-dimensional target vectors t^* are generated using $t_j^* = T_j(x) = \cos(\bar{x} + \phi_j)$, where $\phi_j = -\pi/2 + j\pi/9$ for $j \in [0, 9]$. \bar{x} denotes the mean of x , a 256-dimensional vector whose entries are initialized from a normal distribution with a mean sampled from a uniform distribution between $-\pi$ and π and with a unit variance. The training and test sets respectively contain 5k and 1k examples. The trained network has a 256-100-100-10 topology with tanh hidden and output units, whose forward weights are drawn from a He uniform distribution [31] and zero-initialized for feedback-alignment-based algorithms. The random connectivity matrices of feedback-alignment-based algorithms are drawn from He uniform distributions. The weights are updated after each minibatch of 50 examples, and the network is trained for 500 epochs with a fixed learning rate $\eta = 5 \times 10^{-4}$ for all training algorithms. As this is a regression task, the loss function is the mean squared error. The losses on the training and test sets and the alignment angles with BP updates are monitored every 1k samples. The experiment is repeated 10 times for each training algorithm, with different network initializations for each experiment run.

Dataset	Network	BP	FA	DFA	DRTP
MNIST	FC	5e-2	5e-2	5e-3	1.5e-3
	CONV	5e-2	1.5e-2	5e-3	1.5e-3
CIFAR-10	FC	1.5e-5	1.5e-5	1.5e-5	5e-5
	CONV	1.5e-5	5e-6	1.5e-5	1.5e-4

Table 3: The learning rate values for the MNIST and CIFAR-10 datasets are selected based on a grid search. A different learning rate is chosen for each training algorithm, dataset and network type, i.e. FC or CONV networks (Section 2.4), where Nesterov-accelerated SGD with momentum is the chosen optimizer for MNIST and Adam is the chosen optimizer for CIFAR-10.

Synthetic data classification. The examples in the training and test sets are generated using the `make_classification` function from the Python library `sklearn` [41]. The main inputs required by this function are the number of samples to be generated, the number of features n in the input vectors x , the number of informative features n_{inf} among the input vectors, the number of classes, the number of clusters per class and a factor `class_sep` which conditions the class separation. In this work, we have used $n = 256$ and $n_{inf} = 128$, ten classes, five clusters per class and `class_sep = 4.5`. Using this set of parameters, the `make_classification` function then generates examples by creating for each class clusters of points normally distributed about the vertices of an n_{inf} -dimensional hypercube. The remaining features are filled with normally-distributed random noise. The generated examples are then separated into training and test sets of 25k and 5k examples, respectively. The trained network has a 256-500-500-10 topology with tanh hidden units and sigmoid output units. The forward and backward weights initialization, as well as the forward weight updates, are performed as for regression. As this is a classification task, the loss function is the binary cross-entropy loss. The network is trained for 500 epochs with a fixed learning rate $\eta = 5 \times 10^{-4}$. The losses on the training and test sets and the alignment angles with BP updates are monitored every 2.5k samples. The experiment is repeated 10 times for each training algorithm, with different network initializations for each experiment run.

MNIST and CIFAR-10 images classification. For feedback-alignment-based algorithms, the entries of the fixed random connectivity matrices B_k and of the forward weight matrices W_k are initialized with a He uniform distribution. A fixed learning rate is used to train the network; it is selected based on a grid search for each training algorithm (Table 3). When used, dropout is applied with the same probability to all fully-connected layers. In the MNIST experiments, the networks are trained using stochastic gradient descent (SGD), with a momentum coefficient of 0.9 and with Nesterov accelerated gradients. BP, FA and DRTP are trained with a linear output layer and a cross-entropy loss, which includes a `logsoftmax` operation, while DFA is trained with a sigmoid output layer and a binary cross-entropy loss in order to obtain the highest accuracy for each training algorithm. The networks are trained for 100 epochs with a minibatch size of 60. In the CIFAR-10 experiments, the networks are trained using Adam with default parameters. A sigmoid output layer and a binary cross-entropy loss are used for all training algorithms. A minibatch size of 100 is used and early stopping is applied, with a maximum of 200 epochs. In the experiments with data augmentation, horizontal flips are performed to augment the training set and the maximum number of epochs is increased to 300. For all experiments, the test error is averaged over the last 10 epochs of training and then over the 10 trials conducted for each experiment. Hence, the results reported in Tables 1 and 2 are the mean and standard deviation over the 10 trials.

Acknowledgments

The authors would like to thank Emre Neftci, Giacomo Indiveri, Simon Carbonnelle and Vincent Schellekens for fruitful discussions and Christophe De Vleeschouwer granting access to a deep learning workstation.

C. Frenkel is with Université catholique de Louvain as a Research Fellow from the National Foundation for Scientific Research (FNRS) of Belgium.

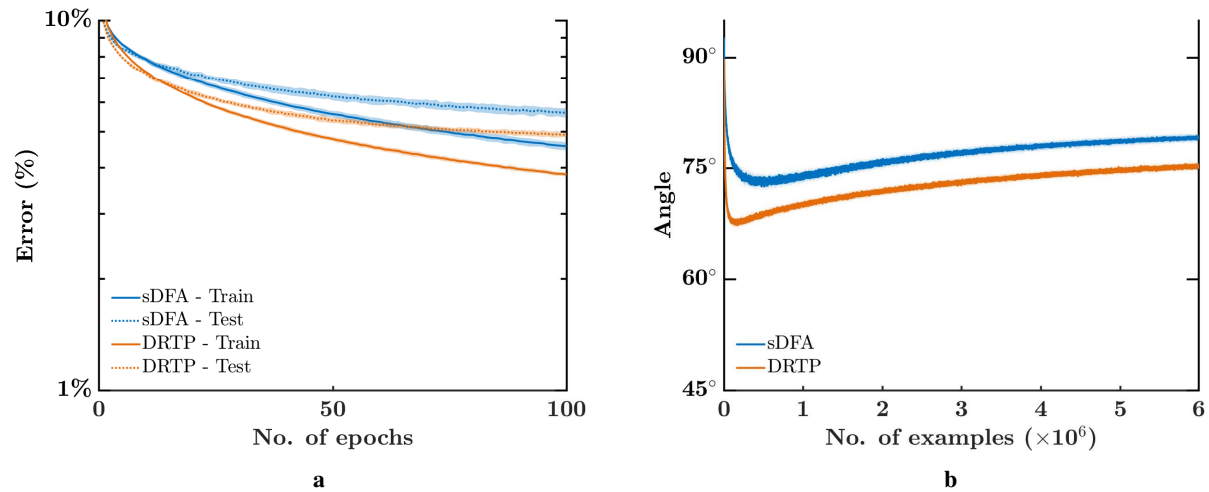
Author Contributions

C.F. developed the main idea. C.F. and M.L. derived the mathematical proofs and worked on the simulation experiments. C.F., M.L. and D.B. wrote the paper.

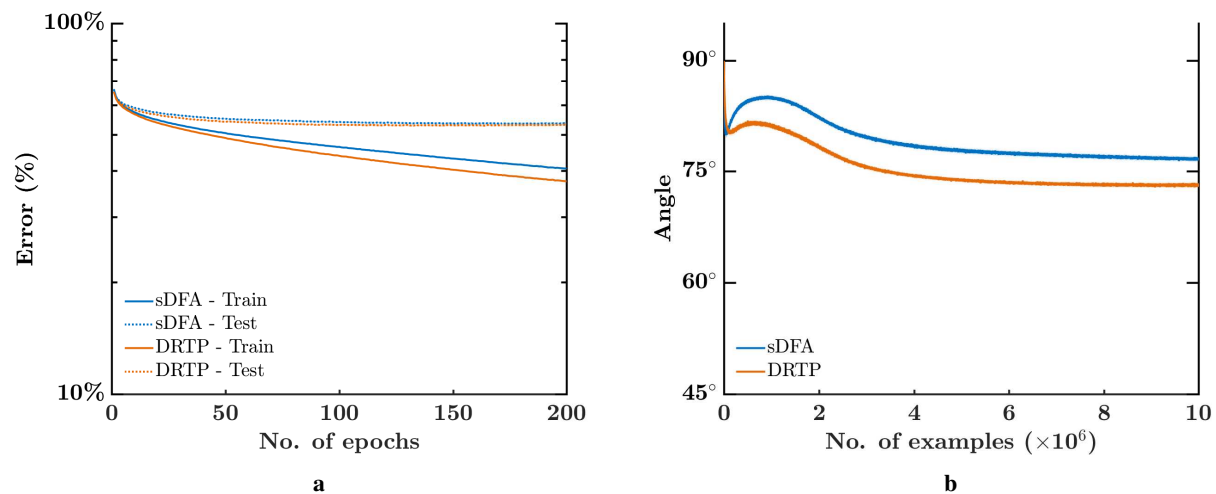
References

- [1] F. Rosenblatt, *Principles of neurodynamics: Perceptrons and the theory of brain mechanisms*, Sparta, NJ, USA: Spartan Books, 1961.
- [2] D. Bassett and E. D. Bullmore, “Small-world brain networks,” *The Neuroscientist*, vol. 12, no. 6, pp. 512-523, 2006.
- [3] M. Minsky, “Steps toward artificial intelligence,” *Proceedings of the IRE*, vol. 49, no. 1, pp. 8-30, 1961.
- [4] D. Rumelhart, G. Hinton and R. Williams, “Learning representations by back-propagating errors,” *Nature*, vol. 323, pp. 533-536, 1986.
- [5] A. Krizhevsky, I. Sutskever and G. E. Hinton, “ImageNet classification with deep convolutional neural networks,” *Proc. of Advances in Neural Information Processing Systems (NIPS)*, pp. 1097-1105, 2012.
- [6] Y. LeCun, Y. Bengio, and G. E. Hinton, “Deep learning,” *Nature*, vol. 521, no. 7553, p. 436, 2015.
- [7] K. He et al., “Deep residual learning for image recognition,” *Proc. of IEEE Conference on Computer Vision and Pattern Recognition (CVPR)*, pp. 770-778, 2016.
- [8] G. E. Hinton et al., “Deep neural networks for acoustic modeling in speech recognition,” *IEEE Signal Processing Magazine*, vol. 29, 2012.
- [9] D. Amodei et al., “Deep speech 2: End-to-end speech recognition in english and mandarin,” *Proc. of International Conference on Machine Learning (ICML)*, vol. 173-182, 2016.
- [10] S. Grossberg, “Competitive learning: From interactive activation to adaptive resonance,” *Cognitive Science*, vol. 11, no. 1, pp. 23-63, 1987.
- [11] Q. Liao, J. Z. Leibo and T. Poggio, “How important is weight symmetry in backpropagation?,” *Proc. of AAAI Conference on Artificial Intelligence*, 2016.
- [12] T. P. Lillicrap et al., “Random synaptic feedback weights support error backpropagation for deep learning,” *Nature Communications*, vol. 7, no. 13276, 2016.
- [13] P. Baldi, P. Sadowski and Z. Lu, “Learning in the machine: Random backpropagation and the deep learning channel,” *Artificial intelligence*, vol. 260, pp. 1-35, 2018.
- [14] A. Nøkland, “Direct feedback alignment provides learning in deep neural networks,” *Proc. of Advances in Neural Information Processing Systems (NIPS)*, pp. 1037-1045, 2016.
- [15] Y. LeCun and C. Cortes, “The MNIST database of handwritten digits,” 1998 [Online]. Available: <http://yann.lecun.com/exdb/mnist/>.
- [16] A. Krizhevsky, *Learning multiple layers of features from tiny images*, Technical Report, University of Toronto, 2009.
- [17] R. Urbanczik and W. Senn, “Learning by the dendritic prediction of somatic spiking,” *Neuron*, vol. 81, no. 3, pp. 521-528, 2014.
- [18] J. Guerguiev, T. P. Lillicrap and A. Richards, “Towards deep learning with segregated dendrites,” *ELife*, vol. 6, no. e22901, 2017.
- [19] E. Neftci et al., “Event-driven random back-propagation: Enabling neuromorphic deep learning machines,” *Frontiers in Neuroscience*, vol. 11, no. 324, 2017.
- [20] M. Jaderberg et al., “Decoupled neural interfaces using synthetic gradients,” *Proc. of International Conference on Machine Learning (ICML)*, vol. 70, pp. 1627-1635, 2017.
- [21] W. Czarnecki et al., “Understanding synthetic gradients and decoupled neural interfaces,” *Proc. of International Conference on Machine Learning (ICML)*, vol. 70, pp. 904-912, 2017.
- [22] H. Mostafa, V. Ramesh and G. Cauwenberghs, “Deep supervised learning using local errors,” *Frontiers in Neuroscience*, vol. 12, no. 608, 2018.
- [23] J. Kaiser, H. Mostafa and E. Neftci, “Synaptic plasticity dynamics for deep continuous local learning,” *arXiv preprint arXiv:1811.10766*, 2018.
- [24] A. Nøkland and L. H. Eidnes, “Training neural networks with local error signals,” *Proc. of International Conference on Machine Learning (ICML)*, 2019.
- [25] J. Deng et al., “ImageNet: A large-scale hierarchical image database,” *Proc. of IEEE Conference on Computer Vision and Pattern Recognition (CVPR)*, pp. 248-255, 2009.

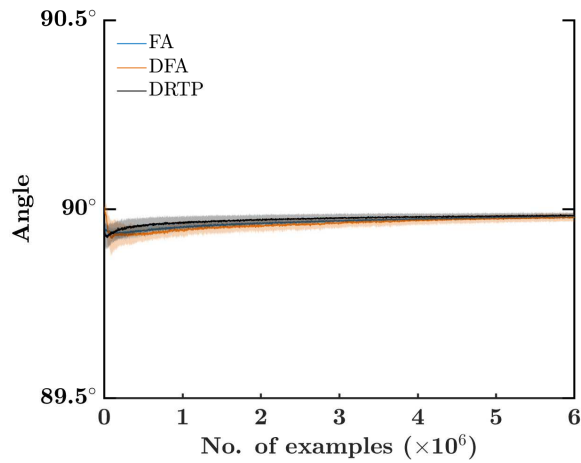
- [26] D. H. Lee et al., “Difference target propagation,” in *Proc. of Springer Joint European Conference on Machine Learning and Knowledge Discovery in Databases*, pp. 498-515, 2015.
- [27] D. Bol, G. de Streel and D. Flandre, “Can we connect trillions of IoT sensors in a sustainable way? A technology/circuit perspective,” *Proc. of IEEE SOI-3D-Subthreshold Microelectronics Technology Unified Conference (S3S)*, 2015.
- [28] M. B. Milde et al., “Obstacle avoidance and target acquisition for robot navigation using a mixed signal analog/digital neuromorphic processing system,” *Frontiers in Neurobotics*, vol. 11, no. 28, 2017.
- [29] C. Frenkel et al., “A 0.086-mm² 12.7-pJ/SOP 64k-synapse 256-neuron online-learning digital spiking neuromorphic processor in 28-nm CMOS,” *IEEE Transactions on Biomedical Circuits and Systems*, vol. 13, no. 1, pp. 145-158, 2019.
- [30] C. Frenkel, J.-D. Legat and D. Bol, “MorphIC: A 65-nm 738k-synapse/mm² quad-core binary-weight digital neuromorphic processor with stochastic spike-driven online learning,” *IEEE Transactions on Biomedical Circuits and Systems*, 2019.
- [31] K. He et al., “Delving deep into rectifiers: Surpassing human-level performance on ImageNet classification,” *Proc. of IEEE International Conference on Computer Vision (ICCV)*, pp. 1026-1034, 2015.
- [32] C. S. Thakur et al., “Large-scale neuromorphic spiking array processors: A quest to mimic the brain,” *Frontiers in Neuroscience*, vol. 12, no. 891, 2018.
- [33] B. Rajendran et al., “Low-Power Neuromorphic Hardware for Signal Processing Applications,” *IEEE Signal Processing Magazine*, 2019.
- [34] G. G. Bi, and M. M. Poo, “Synaptic modifications in cultured hippocampal neurons: Dependence on spike timing, synaptic strength, and postsynaptic cell type,” *Journal of Neuroscience*, vol. 18, no. 24, pp. 10464-10472, 1998.
- [35] J. M. Brader, W. Senn and S. Fusi, “Learning real-world stimuli in a neural network with spike-driven synaptic dynamics,” *Neural Computation*, vol. 19, no. 11, pp. 2881-2912, 2007.
- [36] G. Detorakis et al., “Neural and synaptic array transceiver: A brain-inspired computing framework for embedded learning,” *Frontiers in Neuroscience*, vol. 12, no. 583, 2018.
- [37] J. Park, J. Lee and D. Jeon, “7.6 A 65nm 236.5 nJ/classification neuromorphic processor with 7.5% energy overhead on-chip learning using direct spike-only feedback,” *Proc. of IEEE International Solid-State Circuits Conference (ISSCC)*, pp. 140-142, 2019.
- [38] J. Launay, I. Poli and F. Krzakala, “Principled Training of Neural Networks with Direct Feedback Alignment”, *arXiv preprint arXiv:1906.04554*, 2019.
- [39] F. Zenke, E. J. Agnes and W. Gerstner, “Diverse synaptic plasticity mechanisms orchestrated to form and retrieve memories in spiking neural networks”, *Nature Communications*, vol. 6, no. 6922, 2015.
- [40] A. Paszke et al., “Automatic differentiation in PyTorch”, *31st Annual Conference on Neural Information Processing Systems (NIPS) Workshop*, 2017.
- [41] F. Pedregosa et al., “Scikit-learn: Machine Learning in Python”, *Journal of Machine Learning Research (JMLR)*, vol. 12, pp. 2825-2830, 2011.



Supplementary Figure 1: DRTP outperforms sDFA on the MNIST dataset thanks to a better alignment with the BP loss gradients. Both figures are with error bars of one standard deviation over 10 runs. The training and test errors are measured after of each epoch, while the angle is measured after each minibatch of 60 examples. (a) A 784-1000-10 network with tanh hidden units and sigmoid output units is trained to classify handwritten digits with the sDFA and DRTP algorithms. On average, the error on the training set reaches 4.56% for sDFA and 3.82% for DRTP, while the error on the test set reaches 5.62% for sDFA and 4.90% for DRTP after 100 epochs. (b) While the loss gradients δy_k estimated by both sDFA and DRTP are within 90° of the ones prescribed by BP, the alignment angle is approximately 3.75° better for DRTP than for sDFA.



Supplementary Figure 2: DRTP outperforms sDFA on the CIFAR-10 dataset thanks to a better alignment with the BP loss gradients. Both figures are with error bars of one standard deviation over 10 runs. The training and test errors are measured after of each epoch, while the angle is measured after each minibatch of 100 examples. (a) A 784-1000-10 network with tanh hidden units and sigmoid output units is trained to classify vehicles and animals with the sDFA and DRTP algorithms. On average, the error on the training set reaches 40.74% for sDFA and 37.39% for DRTP, while the error on the test set reaches 53.53% for sDFA and 53.12% for DRTP after 200 epochs. (b) While the loss gradients δy_k estimated by both sDFA and DRTP are within 90° of the ones prescribed by BP, the alignment angle is approximately 3.40° better for DRTP than for sDFA.



Supplementary Figure 3: Updates to the convolutional layer weights prescribed by feedback-alignment-based algorithms are random due to a 90° -alignment with the BP estimated loss gradients δy_k . A convolutional network is trained on the MNIST dataset of handwritten digits with feedback-alignment-based algorithms, i.e. FA, DFA and DRTP. The network topology and training parameters are identical to those used for the trained CONV network in Section 2.4.1. Error bars are one standard deviation over 10 runs, the angle is measured after each minibatch of 60 examples. Angles have been smoothed by an exponentially-weighted moving average filter with a momentum coefficient of 0.95.

Supplementary Note 1. Detailed proof of alignment for the BP and DRTP modulatory signals

This full version of the alignment proof between the BP and DRTP modulatory signals is derived under the assumptions outlined in Section 2.3, i.e. a neural network composed of linear hidden layers (Fig. 4) and a single training example (x, c^*) , where x is the input data sample and c^* the label. The C -dimensional target vector t^* corresponds to the one-hot encoding of c^* , where C is the number of classes. Our developments build on the alignment proof of [12], which demonstrates that the FA and BP modulatory signals are aligned within 90° in the case of a single linear hidden layer, a linear output layer and a mean squared error loss. In the framework of classification problems, we extend it for the case of DRTP and to an arbitrary number of linear hidden layers, a nonlinear output layer of sigmoid units and a binary cross-entropy loss.

Network dynamics. The output of the k -th linear hidden layer is given by

$$y_k = z_k = W_k y_{k-1} \quad \text{for } k \in [1, K-1],$$

where K is the number of layers and $y_0 = x$ is the input vector. The output layer is described by

$$\begin{aligned} z_K &= W_K y_{K-1} \\ y_K &= \sigma(z_K), \end{aligned}$$

where σ is the sigmoid activation function. The loss function $J(\cdot)$ is the binary cross-entropy loss, computed over the C output classes,

$$J(y_K, t^*) = -\frac{1}{C} \sum_{c=1}^C \left(t_c^* \log(y_{Kc}) + (1 - t_c^*) \log(1 - y_{Kc}) \right).$$

The network is trained with stochastic gradient descent. In the output layer, the weight updates of both BP and DRTP follow

$$W_K \leftarrow W_K - \eta \frac{\partial J}{\partial y_K} \frac{\partial y_K}{\partial z_K} \frac{\partial z_K}{\partial W_K}.$$

The factors in this update can be computed as

$$\begin{aligned} \frac{\partial J}{\partial y_{Kc}} &= \begin{cases} -\frac{1}{C} \frac{1}{y_{Kc}} & \text{if } c = c^* \\ -\frac{1}{C} \frac{-1}{(1 - y_{Kc})} & \text{otherwise} \end{cases} \\ \frac{\partial y_K}{\partial z_K} &= y_K (1 - y_K). \end{aligned}$$

It results that

$$\frac{\partial J}{\partial z_K} = \frac{1}{C} (y_K - t^*) = \frac{e}{C},$$

where e is the error vector, and therefore that

$$W_K \leftarrow W_K - \frac{\eta}{C} e y_{K-1}^T.$$

In the hidden layers, the weight updates follow

$$W_k \leftarrow W_k - \eta \delta y_k y_{k-1}^T.$$

On the one hand, if the training relies on the BP algorithm, the modulatory signals $\delta z_k = \delta y_k$ correspond to the loss function gradient:

$$\delta y_k = \delta z_k = \frac{\partial J}{\partial y_k} = \frac{1}{C} \left(\prod_{i=k+1}^K W_i^T \right) e.$$

On the other hand, if the DRTP algorithm is used, the modulatory signals are projections of the one-hot-encoded target vector t^* through fixed random connectivity matrices B_k :

$$\delta y_k = \delta z_k = B_k^T t^*.$$

In order to provide learning, the modulatory signals prescribed by BP and DRTP must be within 90° of each other, i.e. their dot product must be positive:

$$e^T \left(\prod_{i=k+1}^K W_i^T \right)^T B_k^T t^* > 0.$$

Lemma. In the case of zero-initialized weights, i.e. $W_k^0 = 0$ for $k \in [1, K]$, and hence of zero-initialized hidden layer outputs, i.e. $y_k^0 = 0$ for $k \in [1, K-1]$ and $z_K^0 = 0$, considering a DRTP-based training performed recursively with a single element of the training set (x, c^*) and t^* denoting the one-hot encoding of c^* , at every discrete time step t , there are positive scalars $s_{y_k}^t$ and $s_{W_k}^t$ for $k \in [1, K-1]$ and a C -dimensional vector $s_{W_K}^t$ such that

$$\begin{aligned} y_k^t &= -s_{y_k}^t (B_k^T t^*) & \text{for } k \in [1, K-1] \\ W_1^t &= -s_{W_1}^t (B_1^T t^*) x^T \\ W_k^t &= s_{W_k}^t (B_k^T t^*) (B_{k-1}^T t^*)^T & \text{for } k \in [2, K-1] \\ W_K^t &= -s_{W_K}^t (B_{K-1}^T t^*)^T. \end{aligned}$$

Proof. The lemma is proven by induction.

For $t = 0$, the conditions required to satisfy the lemma are trivially met by choosing $s_{y_k}^0, s_{W_k}^0 = 0$ for $k \in [1, K-1]$, and $s_{W_K}^0$ as a zero vector, given that $y_k^0 = 0$ for $k \in [1, K-1]$ and $W_k^0 = 0$ for $k \in [1, K]$.

For $t > 0$, considering that the conditions are satisfied at a given discrete time step t , it must be shown that they still hold at the next discrete time step $t + 1$. In the hidden layers, the weights are updated using the modulatory signals prescribed by DRTP. For the first hidden layer, we have

$$\begin{aligned} W_1^{t+1} &= W_1^t - \eta B_1^T t^* x^T \\ &= -s_{W_1}^t (B_1^T t^*) x^T - \eta (B_1^T t^*) x^T \\ s_{W_1}^{t+1} &= s_{W_1}^t + \eta = s_{W_1}^t + \Delta s_{W_1}^t \end{aligned}$$

and for subsequent hidden layers, i.e. for $k \in [2, K-1]$, we have

$$\begin{aligned} W_k^{t+1} &= W_k^t - \eta B_k^T t^* y_{k-1}^{tT} \\ &= s_{W_k}^t (B_k^T t^*) (B_{k-1}^T t^*)^T + \eta s_{y_{k-1}}^t (B_k^T t^*) (B_{k-1}^T t^*)^T \\ s_{W_k}^{t+1} &= s_{W_k}^t + \eta s_{y_{k-1}}^t = s_{W_k}^t + \Delta s_{W_k}^t. \end{aligned}$$

The weights in the output layer are updated according to the loss function gradient, thus leading to

$$\begin{aligned} W_K^{t+1} &= W_K^t - \frac{\eta}{C} (y_K^t - t^*) y_{K-1}^{tT} \\ &= W_K^t + \frac{\eta}{C} (y_K^t - t^*) s_{y_{K-1}}^t (B_{K-1}^T t^*)^T \\ &= -s_{W_K}^t (B_{K-1}^T t^*)^T + \frac{\eta s_{y_{K-1}}^t}{C} (y_K^t - t^*) (B_{K-1}^T t^*)^T \\ s_{W_K}^{t+1} &= s_{W_K}^t - \frac{\eta s_{y_{K-1}}^t}{C} (y_K^t - t^*). \end{aligned}$$

The output of the first hidden layer is

$$\begin{aligned} y_1^{t+1} &= W_1^{t+1} x \\ &= (W_1^t - \eta B_1^T t^* x^T) x \\ &= \underbrace{W_1^t x}_{y_1^t} - \eta x^T x (B_1^T t^*) \\ &= -s_{y_1}^t (B_1^T t^*) - \eta \|x\|^2 (B_1^T t^*) \\ s_{y_1}^{t+1} &= s_{y_1}^t + \eta \|x\|^2 = s_{y_1}^t + \Delta s_{y_1}^t \end{aligned}$$

and the output of the k -th hidden layer for $k \in [2, K - 1]$ is given by

$$\begin{aligned}
y_k^{t+1} &= W_k^{t+1} y_{k-1}^{t+1} \\
&= -s_{W_k}^{t+1} (B_k^T t^*) (B_{k-1}^T t^*)^T s_{y_{k-1}}^{t+1} (B_{k-1}^T t^*) \\
&= -\left(s_{W_k}^t + \eta s_{y_{k-1}}^t\right) \left(s_{y_{k-1}}^t + \Delta s_{y_{k-1}}^t\right) \|B_{k-1}^T t^*\|^2 (B_k^T t^*) \\
&= -\underbrace{s_{W_k}^t s_{y_{k-1}}^t \|B_{k-1}^T t^*\|^2}_{s_{y_k}^t} (B_k^T t^*) - \left(s_{W_k}^t \Delta s_{y_{k-1}}^t + \eta s_{y_{k-1}}^t \left(s_{y_{k-1}}^t + \Delta s_{y_{k-1}}^t\right)\right) \|B_{k-1}^T t^*\|^2 (B_k^T t^*) \\
s_{y_k}^{t+1} &= s_{y_k}^t + \left(s_{W_k}^t \Delta s_{y_{k-1}}^t + \eta s_{y_{k-1}}^t \left(s_{y_{k-1}}^t + \Delta s_{y_{k-1}}^t\right)\right) \|B_{k-1}^T t^*\|^2 = s_{y_k}^t + \Delta s_{y_k}^t.
\end{aligned}$$

The coefficients $s_{W_1}^t$ and $s_{y_1}^t$ are updated with strictly positive quantities $\Delta s_{W_1}^t$ and $\Delta s_{y_1}^t$ at each time step t and are thus strictly positive for $t > 0$. Furthermore, the coefficients $s_{W_k}^t$ and $s_{y_k}^t$ are updated based on the coefficients of the previous layer and will therefore be strictly positive for $k \in [1, K - 1]$. \square

Theorem. Under the same conditions as in the lemma and for the linear-hidden-layer network dynamics described above, the k -th layer modulatory signals prescribed by DRTP are always a positive scalar multiple of the Moore-Penrose pseudo-inverse of the product of forward matrices of layers $k + 1$ to K , located in the feedback pathway between the output layer and the k -th hidden layer, multiplied by the error. That is, for $k \in [1, K - 1]$ and $t > 0$,

$$\left(\prod_{i=k}^{K-1} W_i^t\right)^+ e = s_k^t B_k^T t^* \quad \text{with } s_k^t > 0.$$

Proof. When replacing the forward weights W_i^t by the expressions given in the lemma, the above equality becomes

$$\begin{aligned}
& - \left[\left(\prod_{i=K-1}^{k+1} s_{W_i}^t\right) s_{W_K}^t \left(\prod_{i=K-1}^{k+1} \|B_i^T t^*\|^2\right) (B_k^T t^*)^T \right]^+ (y_K^t - t^*) = s_k^t B_k^T t^* \\
& - \left(\prod_{i=k+1}^{K-1} s_{W_i}^t\right)^{-1} \left(\prod_{i=k+1}^{K-1} \|B_i^T t^*\|^2\right)^{-1} \left[s_{W_K}^t (B_k^T t^*)^T\right]^+ (y_K^t - t^*) = s_k^t B_k^T t^* \\
& - \left(\prod_{i=k+1}^{K-1} s_{W_i}^t\right)^{-1} \left(\prod_{i=k+1}^{K-1} \|B_i^T t^*\|^2\right)^{-1} (B_k^T t^*)^{T+} s_{W_K}^{t+} (y_K^t - t^*) = s_k^t B_k^T t^* \\
& - \left(\prod_{i=k+1}^{K-1} s_{W_i}^t\right)^{-1} \left(\prod_{i=k+1}^{K-1} \|B_i^T t^*\|^2\right)^{-1} \underbrace{\|B_k^T t^*\|^{-2} (B_k^T t^*)}_{(B_k^T t^*)^{T+}} \underbrace{\|s_{W_K}^t\|^{-2} s_{W_K}^{tT}}_{s_{W_K}^{t+}} (y_K^t - t^*) = s_k^t B_k^T t^* \\
& - \left(\prod_{i=k+1}^{K-1} s_{W_i}^t\right)^{-1} \left(\prod_{i=k}^{K-1} \|B_i^T t^*\|^2\right)^{-1} \|s_{W_K}^t\|^{-2} s_{W_K}^{tT} (y_K^t - t^*) (B_k^T t^*) = s_k^t (B_k^T t^*).
\end{aligned}$$

By identification, it is found that

$$s_k^t = \frac{-s_{W_K}^{tT} (y_K^t - t^*)}{\left(\prod_{i=k+1}^{K-1} s_{W_i}^t\right) \left(\prod_{i=k}^{K-1} \|B_i^T t^*\|^2\right) \|s_{W_K}^t\|^2}.$$

Moreover, the update formula for the vector $s_{W_K}^t$ is given by

$$s_{W_K}^{t+1} = s_{W_K}^t - \frac{\eta s_{y_{K-1}}^t}{C} (y_K^t - t^*),$$

where η , C and $s_{y_{K-1}}^t$ are positive scalars. As shown in Section 2.2, for any example (x, c^*) in the training set, the error vector $e = (y_K - t^*)$ has a single strictly negative entry $(y_{Kc} - 1)$ at the class label index $c = c^*$, all the other entries

y_{Kc} with $c \neq c^*$ being strictly positive. This sign information is constant as the network is trained with a single training example. Given that $s_{W_K}^0 = 0$ from zero-weight initialization and that $s_{W_K}^t$ is updated in a direction opposite to that of e , we have at every discrete time step t

$$\text{sign}(s_{W_K}^t) = -\text{sign}(y_K^t - t^*),$$

and thus

$$-s_{W_K}^{tT} (y_K^t - t^*) > 0.$$

Therefore, the scalars s_k^t are strictly positive for $t > 0$. □

Alignment. In the framework of classification problems, as the coefficients s_k^t are strictly positive scalars for $t > 0$, it results from the theorem that the dot product between the BP and DRTP modulatory signals is strictly positive, i.e.

$$\begin{aligned} e^T \left(\prod_{i=k+1}^K W_i^T \right)^T (B_k^T t^*) &> 0 \\ e^T \underbrace{\left(\prod_{i=k+1}^K W_i^T \right)^T \left(\prod_{i=K}^{k+1} W_i \right)^+}_I \frac{e}{s_k^t} &> 0 \\ \frac{e^T e}{s_k^t} &> 0. \end{aligned}$$

The BP and DRTP modulatory signals are thus within 90° of each other. □